INSTITUT DE FRANCE
Académie des sciences

Comptes Rendus

Chimie

Michel Daudon, Margaux Petay, Sophie Vimont, Ariane Deniset, Frederik Tielens, Jean-Philippe Haymann, Emmanuel Letavernier, Vincent Frochot and Dominique Bazin

Urinary tract infection inducing stones: some clinical and chemical data

Volume 25, Special Issue S1 (2022), p. 315-334

Published online: 15 March 2022

https://doi.org/10.5802/crchim.159

Part of Special Issue: Microcrystalline pathologies: Clinical issues and nanochemistry

Guest editors: Dominique Bazin (Université Paris-Saclay, CNRS, ICP, France), Michel Daudon, Vincent Frochot, Emmanuel Letavernier and Jean-Philippe Haymann (Sorbonne Université, INSERM, AP-HP, Hôpital Tenon, France)

Les Comptes Rendus. Chimie *sont membres du*
Centre Mersenne pour l'édition scientifique ouverte
www.centre-mersenne.org
e-ISSN : 1878-1543

Comptes Rendus
Chimie
2022, Vol. 25, Special Issue S1, p. 315-334
https://doi.org/10.5802/crchim.159

Microcrystalline pathologies: Clinical issues and nanochemistry / *Pathologies microcristallines : questions cliniques et nanochimie*

Urinary tract infection inducing stones: some clinical and chemical data

Michel Daudon[*, a, b, c], **Margaux Petay**[d], **Sophie Vimont**[b, c, e], **Ariane Deniset**[d], **Frederik Tielens**[f], **Jean-Philippe Haymann**[a, b, c], **Emmanuel Letavernier**[a, b, c], **Vincent Frochot**[a, b, c] **and Dominique Bazin**[d, g]

[a] Explorations fonctionnelles multidisciplinaires, AP-HP, Hôpital Tenon, Paris, France

[b] Sorbonne Universités, UPMC Univ Paris 6, UMR S 1155, Paris, France

[c] INSERM, UMR S 1155, Paris, France

[d] Institut de Chimie Physique, UMR CNRS 8000, Bâtiment 350, Université Paris Saclay, 91405 Orsay cedex, France

[e] Département de bactériologie, AP-HP, Hôpital Saint-Antoine, Paris, France

[f] Eenheid Algemene Chemie (ALGC) – Materials Modelling Group, Vrije Universiteit Brussel (VUB), Pleinlaan 2, 1050 Brussel, Belgium

[g] Laboratoire de Physique des Solides, UMR CNRS 8502, Bâtiment 510, Université Paris Saclay, 91405 Orsay cedex, France

E-mails: daudonmichel24@gmail.com (M. Daudon), margaux.petay@universite-paris-saclay.fr (M. Petay), sophie.vimont@aphp.fr (S. Vimont), ariane.deniset@universite-paris-saclay.fr (A. Deniset), frederik.tielens@vub.be (F. Tielens), jean-philippe.haymann@aphp.fr (J.-P. Haymann), emmanuel.letavernier@aphp.fr (E. Letavernier), vincent.frochot@aphp.fr (V. Frochot), dominique.bazin@universite-paris-saclay.fr (D. Bazin)

Abstract. Most papers on kidney stones arising from infection concentrate on the mineral struvite. In this contribution, we would like to call attention to other mineral phases such as highly carbonated calcium phosphate apatite, ammonium urate, and whitlockite, by presenting clinical and chemical data. We start with epidemiological data which emphasize the increase in the prevalence of kidney stones related to infection. Then we present a statistical analysis of more than 85,000 stones which have been analysed at the Laboratoire des Lithiases of Assistance Publique-Hôpitaux de Paris which gives insights regarding the link between urinary tract infection and struvite, carbonated calcium phosphate apatite (carbapatite), and also surprisingly whitlockite. Some information regarding the pathogenesis of kidney stones linked to infection, the nature of the bacteria which have been identified, and the approach to precisely analyse infrared spectra to identify struvite, carbapatite, and whitlockite, conclude this first part. To complete this clinical description, we describe the crystallographic structure and the chemistry of three relevant compounds namely carbonated calcium phosphate, struvite, and whitlockite. To conclude this second part, the dependence of crystallite morphology of struvite on pH and on the presence, or absence, of bacteria, is described. Based on clinical and

* Corresponding author.

chemical data, it is becoming clear that struvite is not the only mineral intimately related to renal infectious processes, but that whitlockite and carbapatite with a high carbonation rate are strongly associated with urinary tract infection as well.

Keywords. Infection-induced calculi, Struvite, Whitlockite, Amorphous carbonated calcium phosphate, Carbapatite, Carbonation rate, Urease-splitting bacteria.

Published online: 15 March 2022

1. Introduction

Urinary tract infections (UTI), ranging from uncomplicated cystitis to severe pyelonephritis and nephrolithiasis, are the third most common type of infection in human medicine (after respiratory and alimentary infections), affecting 150 million people each year worldwide [1,2]. As reported by Flores-Mireles *et al.* [3], the societal costs of these infections, including health care costs and time missed from work, are approximately US$3.5 billion per year in the United States alone.

Regarding clinical presentation, UTI is associated with flank or abdominal pain (70%), typical renal colic (rare), fever (26%), gross haematuria (18%), and sepsis (1%), but can be asymptomatic (8%—incidental diagnosis). Infection of the urinary system may lead to the formation of concretions [4–9] as well as an incrustation of JJ stents [10–13]. It is well known that infection stones form secondary to urease-splitting organisms such as *Proteus*, *Klebsiella*, *Pseudomonas*, or *Staphylococcus*, among others. With elevated urine pH due to infection of the urinary tract, the patient becomes prone to form magnesium ammonium phosphate hexahydrate (MAP or struvite), carbonated calcium phosphate apatite (carbapatite or CA), or amorphous carbonated calcium phosphate (ACCP) stones [14,15].

It is worth noting that while infection can initiate the stone, it can also contribute to the progression of a pre-existing metabolic stone: in practice, the reality is undoubtedly more complex. Letavernier [16] suggests that a urinary metabolic anomaly such as hypercalciuria could favour crystallization of calcium phosphate in the presence of non-ureasic bacteria like *Escherichia coli*. It is a new concept in addition to classical situations described by Miano *et al.* [17] which consider two different clinical pictures: stones that develop following UTI, and stones complicated by UTI (stones with infection) which are metabolic stones that passively trap bacteria from coexistent UTIs and may or may not contain calcium.

This short review provides an overview of infection kidney stones (IKS) and treats both clinical and chemical data. We will start by considering epidemiologic data which indicate a significant increase in the prevalence of IKS. Thanks to the data bank from the Laboratoire des Lithiases of Assistance Publique-Hôpitaux de Paris which details the chemical composition of kidney stones determined by Fourier Transform InfraRed (FTIR) spectroscopy [18,19] as well as clinical data from more than 85,000 patients, we will establish a significant relationship between UTI and different chemical compounds namely MAP, CA, ACCP and whitlockite (Wk). Information on the pathogenesis of IKS as well as the nature of the bacteria identified in the patients concludes this section. To complete this clinical description, the crystallographic structure and chemistry of three chemical compounds, namely MAP, CA and Wk, are presented, concluding with descriptions of crystallite morphology of these three chemical phases in the presence or absence of bacteria.

2. Clinical data regarding IKS

2.1. *Some epidemiological data*

In developing countries, major differences in the incidence of infection stones have been observed depending on continent and region, from 2.7% in Asia Minor to 13% in South America and 42.9% in Sub-Saharan Africa. These differences reflect the infectious risk factors specific to certain populations, such as nutrition and availability of modern medicine and antibiotics in each specific area [20].

Considering all criteria from stone analysis suggestive of infection-related stones, we and others [18, 21,22] in industrialized countries observed a decrease of infection stones over several decades before 2000, but a constant increase in the proportion of stones related to infection in both sexes thereafter (Figure 1). Such a significant increase may be due to different factors such as the evolution of bacteria resistant to antibiotics, or more limited access to medicine. Of note, the relative proportion of UTI

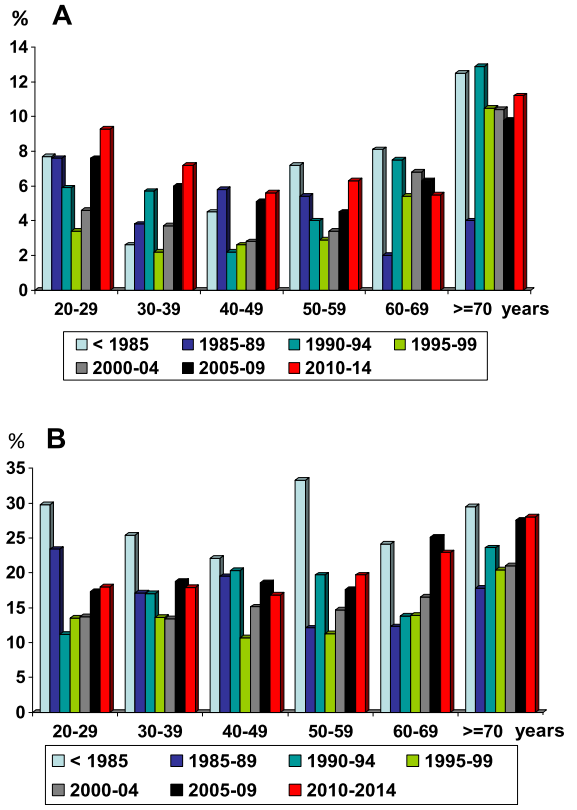

Figure 1. Evolution of infection stones in humans as a function of age and time period: A = men; B = women (from Ref. [18]). After a constant decrease in the proportion of infection stones in the second part of the twentieth century, we observed a new increase of infection stones at the beginning of the twenty-first century.

stone occurrence in men ranged from 3.2 to 10.1% and was slightly higher at the extremes of life [21]. As shown in Figures 1A and B, infection stones occur more frequently in female than in male patients across all ages.

2.2. *Chemical phases related to clinically indicated UTI*

Each stone sent for analysis in our lab is accompanied by an information sheet including anthropometric and clinical data. A clinically symptomatic urinary tract infection is one of the queries. Based on the data bank, the relationship between UTI and the main chemical compound present in the chemical composition of the stones removed from patients is summarized in Table 1. Consistent with the literature, the first compound in Table 1 is struvite, considered as a strong marker of this lithogenic process [23–30]. We note surprisingly that UTI was clinically identified in only 65.8% of cases where the stone contains any proportion of struvite. The link is slightly stronger for stones mainly composed of struvite (71.2%).

The statistical analysis (Table 1) clearly implicates a new compound as strongly related to UTI, namely Wk. Actually, more than 50% of patients with whitlockite stones had clinically recognized UTI. Such a result is in line with previous publications in which the content of Wk in kidney stones greater than 20%, estimated by FTIR, was related to infection with a high degree (80% of cases) [31]. Such relationship has been found also in a recent publication dedicated to Wk [32].

Considering CA, we also found a relationship between this compound and UTI. More precisely, we have previously noticed a significant association between a high CO_3^{2-}/PO_4^{3-} ratio in CA, and both the presence of ACCP as determined by FTIR, and the presence of bacterial imprints as shown by scanning electron microscopy (SEM) [33–37]. Ammonium urate (AmUr) is another chemical compound in Table 1 related to UTI [36–38]. Quite recently, Chou *et al.* [39] have noticed that comorbidities of ammonium acid urate urolithiasis stones included chronic kidney disease (60%), UTI (52%), irritable bowel syndrome (36%), and gout (28%). For stones composed of the other compounds, namely brushite (Br), cystine (CYS), uric acid, or calcium oxalates, less than 25% of patients had a urinary tract infection ($p < 10^{-3}$).

While MAP, Wk, and apatite have been identified in concretions at the surface of JJ stents, it seems that Wk is quite rare among the chemical phases present. Indeed, in a recent study on the mechanical properties of used JJ stents [40–42], chemical analysis of the calcifications at the surface of 52 stents shows the presence of different chemicals including ACCP, CA, Br, octacalcium phosphate pentahydrate (OCP), MAP, AmUr, weddellite (calcium oxalate dihydrate or COD), whewellite (calcium oxalate monohydrate or COM), CYS, mucopolysaccharides (MPS), proteins (PRO), and triglycerides (TRG), but no Wk. Such chemical specificity for the JJ stent is confirmed by a statistical study based on 1676 JJ stents char-

Table 1. Relationship between UTI and the chemical composition of stones determined by FTIR spectroscopy

Main crystalline or amorphous phase	Number of UTI*	Number of patients without recognized UTI	Occurrence of UTI (%)
Struvite	477	193	71.2[d]
Wk	35	31	53.0[a,c,e]
ACCP	21	20	51.2[a]
CA with CO_3 rate ≥ 15%	354	323	52.3[a,d]
OCP	21	42	33.3
CA (overall)	1024	2276	31.0[b]
AmUr	27	62	30.3[b]
Brushite	160	579	21.7[g]
UA0	542	2558	17.5
CYS	89	427	17.3
UA2	47	402	10.5[f]
COM	1900	16,675	10.2
COD	613	7148	7.9
Total	4956	30,413	14.0

*UTI was defined as UTI clinically diagnosed on the basis of urine culture and biological signs in patients.

COM = calcium oxalate monohydrate, COD = calcium oxalate dihydrate, Cys = cystine, OCP = octacalcium phosphate pentahydrate, UA0 = uric acid anhydrous, UA2 = uric acid dihydrate.

[a] $p < 0.01$ vs MAP; [b] $p < 10^{-6}$ vs MAP.

[c] $p < 0.001$ vs CA; [d] $p < 10^{-6}$ vs CA.

[e] $p < 10^{-6}$ vs metabolic compounds (UA0, UA2, CYS, COM, COD).

[f] $p < 0.001$ vs AU0.

[g] $p < 10^{-4}$ vs Wk, UA2, COM, COD.

acterized at the Crystal Laboratory of Tenon Hospital; only one device had Wk as a major component, and Wk was present in 26 other stents. These observations correspond to 1.6% of cases, while in kidney stones the occurrence of Wk is equivalent to 4.4%. Note that, in the case of MAP, the same percentage is observed for both kidney stones and the JJ stent i.e. 7.2% [37].

2.3. *Pathogenesis of IKS*

The literature indicates clearly that the pathogenesis of IKS is the consequence of a high urine pH and of the production of NH_4^+ ions as a result of urea hydrolysis by bacterial urease [5,9,43,44]. As noted by Konieczna *et al.* [45], urease (urea amidohydrolase) was the first enzyme to be crystallized (1926). It was also the first enzymatic protein in which nickel ions were observed [46].

Hydrolysis of urea by urease is a complex process [45]. The first step generates one molecule of ammonia and one of carbamate appears. In aqueous solution, carbamate spontaneously converts into the second ammonia molecule and carbonic acid. Protonation of ammonia (Figure 2) results in a pH increase.

High urine pH also results in an increased calcium phosphate supersaturation, which facilitates the formation of insoluble salts such as CA and ACCP (Figure 3). However, other changes of urine biochemistry result from ureolysis, such as an increase in CO_3^{2-} ions that may end up incorporated within CA and ACCP structures.

As Figure 3 shows, four chemical phases com-

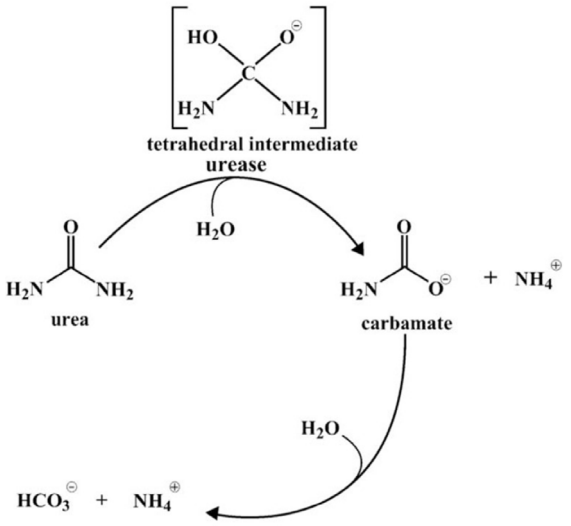

Figure 2. Mechanism of urea hydrolysis (Konieczna *et al.* [45]).

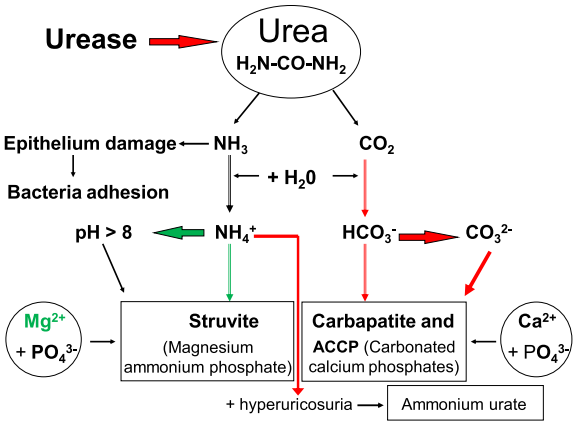

Figure 3. Pathogenesis of infection stones induced by urease-producing bacteria.

monly occur, namely struvite, ACCP, CA and AmUr. Other chemical phases may be present in IKS but an agglomeration of small crystallites trapped in the biofilm produced by bacteria could be an explanation of the presence of these, which may be related to other metabolic disorders as well.

From a clinical point of view, one cannot completely exclude the possibility of struvite stones related to conditions other than UTI if urine biochemistry is similar (for other pathological reasons) to that produced by urea-splitting bacteria. To date, no reports of such conditions have appeared in humans. Thus, our discussion of the potential link between UTI and various crystalline phases identified in urinary calculi will omit any unsubstantiated causes of struvite formation.

2.4. *Nature of the bacteria related to UTI*

As reported in several publications [47–51], the most common pathogens in UTI are the members of the Enterobacterales order (Gram-negative bacteria found in the gut, namely *Escherichia coli*, *Klebsiella* spp., pathogens of the CES group (*Citrobacter–Enterobacter–Serratia*), members of the Proteae tribe (*Proteus–Providencia–Morganella*) with a very high proportion of urease-positive strains; other causative agents include Gram-positive cocci (*Enterococcus* spp., *Streptococcus* spp., *Staphylococcus saprophyticus*, *Staphylococcus epidermidis* and *Staphylococcus aureus*), non-fermenting Gram-negative bacteria (*Pseudomonas* spp. and *Acinetobacter* spp.), atypical microorganisms (*Mycoplasma*, *Ureaplasma* species) and yeasts (*Candida* spp.).

A generally urease negative species is *Escherichia coli*, among strains of which only about 1% of urease-positive isolates were found. In Table 2 we summarize the main micro-organisms identified in urine samples from 980 patients of our cohort with urinary stones containing any proportion of MAP. Urea-splitting bacteria were most frequent (72.0%).

Table 3 shows that the distribution of micro-organism strains in urine from patients who have formed Wk-containing stones is different from that observed for MAP stones.

3. Infrared spectroscopy identification of MAP and Wk

Infrared spectroscopy is one of the most common physical techniques used for stone analysis [52–60]. An infrared spectrum can be considered as the fingerprint of a compound or a mixture of several components in various proportions. However, because minerals, in particular phosphate compounds, exhibit broad peaks and are often present as mixtures in the same stone, it may sometimes be difficult to identify each crystalline phase accurately.

However, for clinical purposes, it is very important to detect the presence of certain components such as

Table 2. Microorganisms identified in urine of stone formers with MAP-containing calculi

Bacterial strain	Number of cases	%	Urease
Proteus mirabilis	528	53.9	+
Escherichia coli	188	19.2	−
Pseudomonas aeruginosa	53	5.4	+
Enterococcus faecalis	48	4.9	−
Klebsiella pneumoniae	42	4.3	+
Staphylococcus aureus	29	3.0	+
Enterobacter cloacae	25	2.6	−
Staphylococcus epidermidis	15	1.5	+
Corynebaterium urealyticum	13	1.3	+
Serratia marcescens	7	0.7	+
Citrobacter freundii	7	0.7	−
Candida albicans	6	0.6	−
Morganella morganii	5	0.5	+
Providencia stuartii	4	0.4	+
Proteus vulgaris	4	0.4	+
Staphylococcus saprophyticus	4	0.4	+
Ureaplasma urealyticum	2	0.2	+
Total	980	100.0	

Table 3. Occurrence of micro-organisms identified in urine samples from patients who form stones without MAP

Bacterial strain	Patients with Wk-containing stones		Patients with stones without Wk		p vs Wk stones
	Number	%	Number	%	
Proteus mirabilis	20	11.8	134	10.7	NS
Escherichia coli	99	58.6	632	50.2	NS
Pseudomonas aeruginosa	24	14.2	83	6.6	0.001
Enterococcus faecalis	7	4.1	124	9.9	NS
Klebsiella pneumoniae	7	4.1	68	5.4	NS
Staphylococcus sp.	5	3.0	88	7.0	NS
Enterobacter cloacae	2	1.2	24	1.9	NS
Corynebaterium sp.	3	1.8	3	0.2	
Citrobacter freundii	2	1.2	16	1.2	NS
Candida albicans	—	—	21	1.7	
Others	—	—	65	5.2	—
Total	169	100.0	1258	100.0	

MAP or Wk that may be markers for urinary tract infection as the cause of the stone. When MAP is the main component, it is easy to identify as shown in the infrared spectrum of pure struvite in Figure 4. Its main characteristics are a very strong ν_3 PO_4^{3-} vibration at 1005 cm^{-1} with a strong and broad absorp-

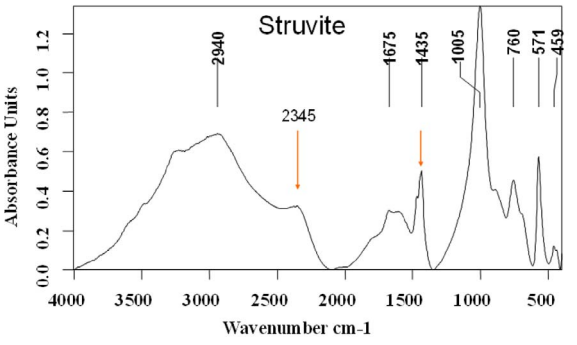

Figure 4. Struvite infrared spectrum.

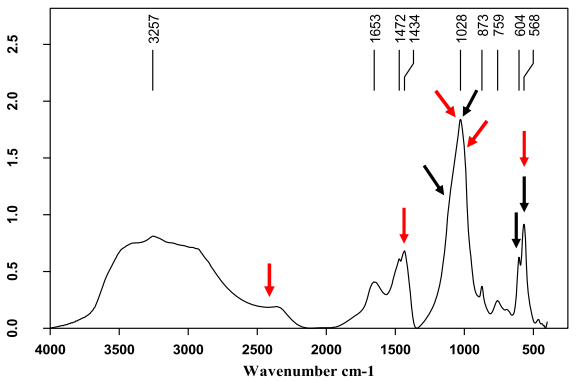

Figure 5. Mixed struvite (red arrows) and calcium phosphate (black arrows) stone.

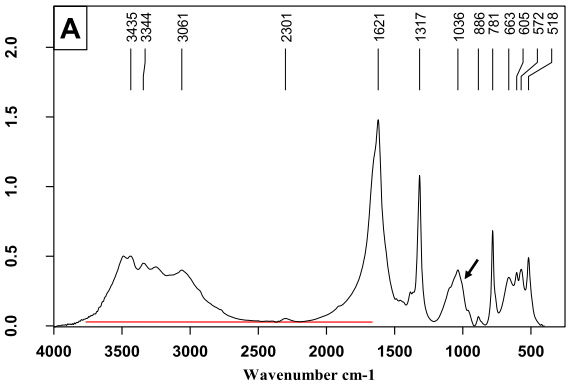

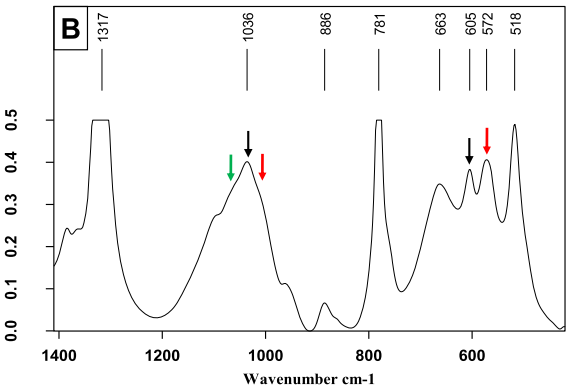

Figure 6. Mixed calcium stone mainly containing calcium oxalate monohydrate with small proportions of ACCP (green arrow), CA (black arrows) and MAP (red arrows). (A) FTIR spectrum on the wavenumber range 4000–400 cm^{-1}. (B) Enlargement of a portion of Figure 6A to better see the shoulders on the broad ν_3 phosphate band.

tion between 3700 and 2100 cm^{-1} due to ν_3 stretching vibrations of hydrogen peaks of the six water molecules and of the $NH4^+$ group, with a decrease on the right side as a pseudo-plateau between 2500 and 2345 cm^{-1} [61,62]. Another interesting vibration is the ν_2 bending peak of the ammonium group at 1435 cm^{-1}. Finally, a ν_2 peak of the PO_4^{3-} group can be observed at 571 cm^{-1}. Note that ν_2 and ν_4 bending vibrations of water molecules can be seen at 1675 and 760 cm^{-1} respectively.

When MAP is a minor component in a phosphate mixture, it is of prime importance to detect its infrared bands, mainly the plateau at 2345 cm^{-1}. The ν_2 peak of NH_4^+ is also relevant. In the case of very common mixtures of MAP with carbonated calcium phosphates, it is often shifted on the right side due to its association with the ν_3 stretching band of the CO_3^{2-} group. Finally, the ν_3 PO_4^{3-} peak of MAP can be obscured by the broad ν_3 PO_4^{3-} peak of other phosphates between 1020 and 1040 cm^{-1}.

As shown in Figure 5, in calcium orthophosphate mixtures containing less than 30% MAP, the pseudo-plateau arising at 2345 cm^{-1} is less intense, the ν_3 PO_4^{3-} peak at 1035–1030 cm^{-1} is slightly shifted towards lower wavenumbers and the edge of the peak to the right is a discrete shoulder at about 1005 cm^{-1} (red arrows).

The same criteria can be useful when MAP is only present as a small proportion of the mixture. For example, the spectrum in Figure 6 mainly shows whewellite (calcium oxalate monohydrate), carbapatite (10%), and struvite (≤5%). Note that the pseudo-plateau between 2500 and 2345 cm^{-1} is only very slightly above the baseline at 2100–

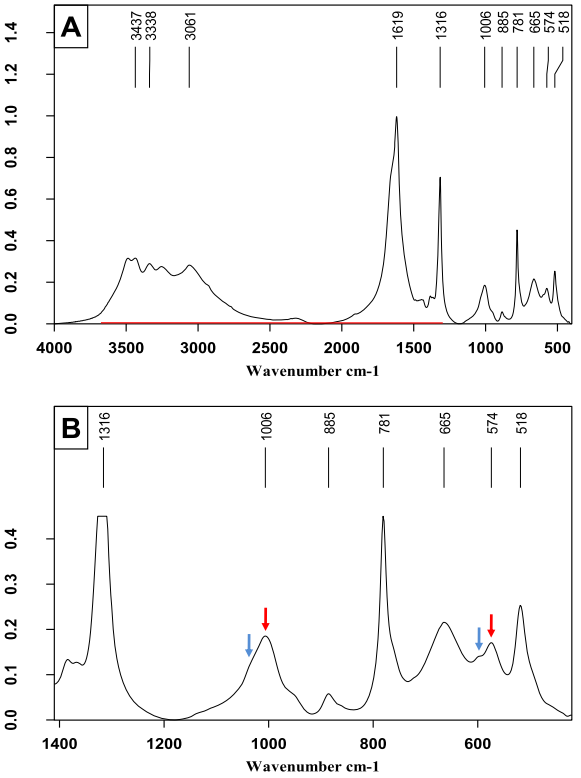

Figure 7. Another mixed stone containing struvite. (A) FTIR spectrum on the wavenumber range 4000–400 cm^{-1}. Note the presence of a plateau between 2500 and 2345 cm^{-1} indicative of struvite. (B) Enlargement of a portion of Figure 7A to see more easily some details of the phosphate bands. Shoulders at 1035 and 600 cm^{-1} correspond to CA bands (blue arrows) while peaks at 1006 and 574 cm^{-1} (red arrows) correspond to struvite. Other peaks indicate the presence of calcium oxalate monohydrate.

2150 cm^{-1}. However, other markers of MAP can be used such as the discrete shoulder at 1005 cm^{-1} (black arrow) and that to the left of the ν_4 PO_4 peak at 572 cm^{-1} (red arrow on the expanded spectrum in Figure 6B).

The expanded spectrum (Figure 6B) reveals a third phosphate, namely ACCP, detected by the slight convexity (green arrow) between the ν_3 PO_4^{3-} peak of carbapatite at 1036 cm^{-1} and its left-hand shoulder at 1097 cm^{-1} [63,64].

The final spectrum (Figure 7) shows a mainly

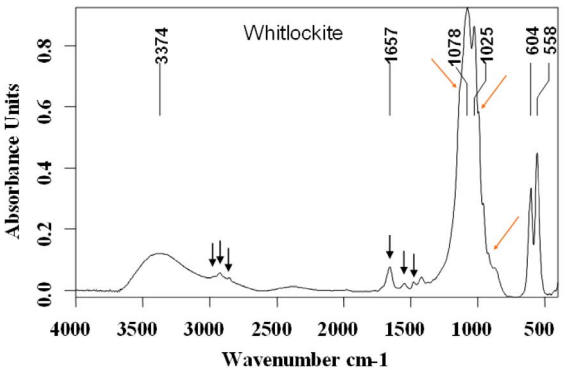

Figure 8. Whitlockite infrared spectrum.

whewellite composition, with struvite content less than 15%. The pseudo-plateau at 2345 cm^{-1} is more prominent and the ν_3 PO_4^{3-} peak at 1005–1006 cm^{-1} is not shifted, due to a very low proportion of calcium phosphates.

Nevertheless, the spectrum expansion in Figure 7B reveals shoulders due to the presence of CA (blue arrows) on the left of the struvite peaks. CA accounted for less than 10% of the mixture.

Whitlockite is another compound often related to urinary tract infection. Its infrared spectrum is shown in Figure 8 where a small proportion of proteins may also be detected (black arrows).

Characteristic vibrations for Wk are observed as a strong band with two maxima at 1078 (ν_3 HPO_4^{2-}) and 1025 (ν_3 PO_4^{3-}) cm^{-1} with shoulders at 1135 and 990 cm^{-1} (red arrows). A third shoulder can be observed at 922 cm^{-1} (red arrow). Note the peak at 1078 cm^{-1} is more intense than the one at 1025 cm^{-1}. The ν_2 and ν_4 PO_4^{3-} bending vibrations are observed at 603 and 558 cm^{-1}.

As with MAP, Wk is rarely the only phosphate present. It is almost always accompanied by CA. In such cases, the ν_4 PO_4^{3-} band of Wk at 558 cm^{-1} is slightly shifted above 560 cm^{-1}. Thus Figure 9 shows an infrared spectrum where whewellite is the main component accompanied by a small proportion of Wk (about 7–8%) and of CA (≤5%).

In cases where CA is the main component (Figure 10), it is of prime importance to look for other phosphates and particularly Wk. For this purpose, one must detect a shoulder at 990 cm^{-1} to the right of the ν_3 stretching band of CA and another shoulder to its left side at about 1135 cm^{-1}

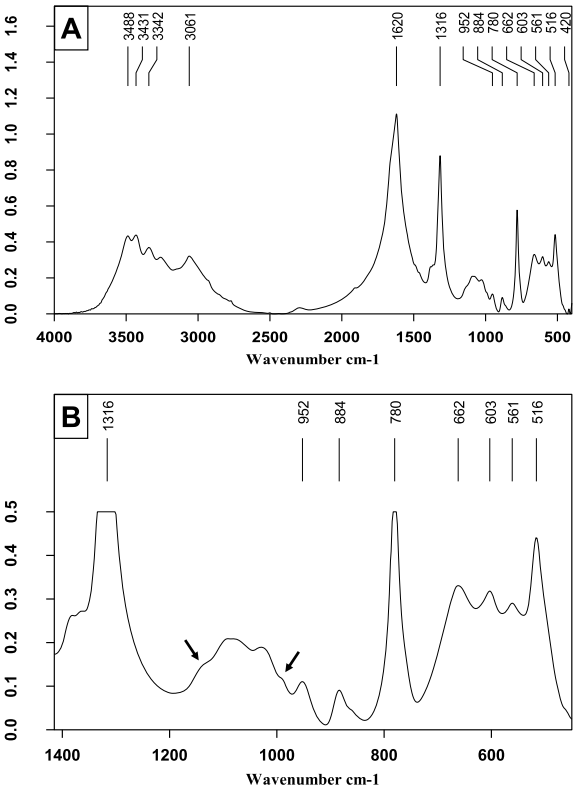

Figure 9. Kidney stone mainly containing whewellite accompanied by a small proportion of whitlockite (about 7–8%) and of carbapatite (less than 5%). (A) FTIR spectrum on the wavenumber range 4000–400 cm^{-1}. (B) Enlargement of a portion of Figure 9A to better see some details of the phosphate bands: shoulders of the whitlockite at 1135 and 991 cm^{-1} are marked by the black arrows.

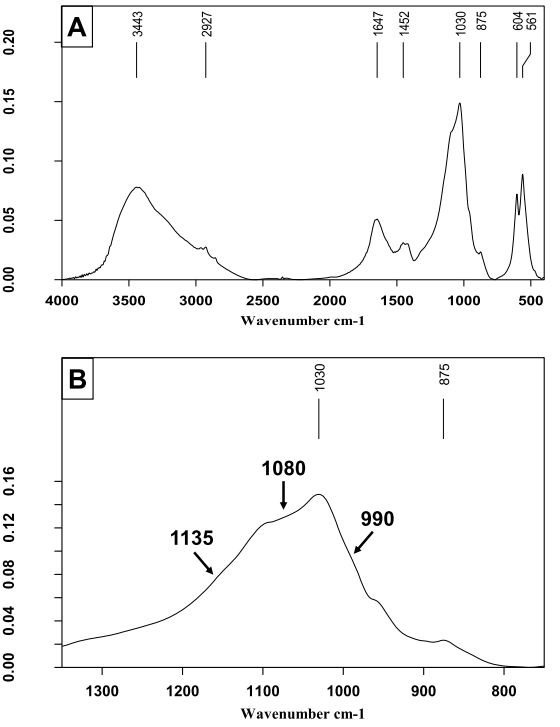

Figure 10. Carbapatite and whitlockite stone. (A) FTIR spectrum on the wavenumber range 4000–400 cm^{-1}. (B) Enlargement of a portion of Figure 10A to see some details of the phosphate bands, especially shoulders of whitlockite at 1135 and 990 cm^{-1}.

(see the expanded spectrum). Note that, in addition, the spectrum shows a small proportion of proteins (ν_3 C–H stretching bands between 2860 and 2960 cm^{-1}).

4. Physicochemical data regarding IKS

4.1. *Crystallographic structure of chemical phases related to infection*

4.1.1. *Struvite*

This compound was named after Heinrich Christoph Gottfried von Struve (1772–1851) of the Russian diplomatic service who was a co-founder of a natural science museum in Hamburg. Struvite ($MgNH_4PO_4{\cdot}6H_2O$), a white inorganic crystalline mineral, crystallizes in the orthorhombic system with cell dimensions $a = 6.941 \pm 0.002$ Å, $b = 6.137 \pm 0.002$ Å, $c = 11.199 \pm 0.004$ Å. The space group is $Pmn2_1$ and there are two molecules in the unit cell [65–70]. Figure 11A shows the atomic scale structure of struvite and Figure 11B the morphology of the struvite crystal [68]. As we will see, struvite may present very different morphologies.

4.1.2. *Carbapatite*

The mineral's name is derived from the Greek word $\alpha\pi\alpha\tau\epsilon\acute{\iota}\nu$ (apatein), which means to deceive or to be misleading. The crystallographic structure of calcium phosphate hydroxyapatite (HAP) is well known. The space group is $P6_3/m$ (Figure 12A), the

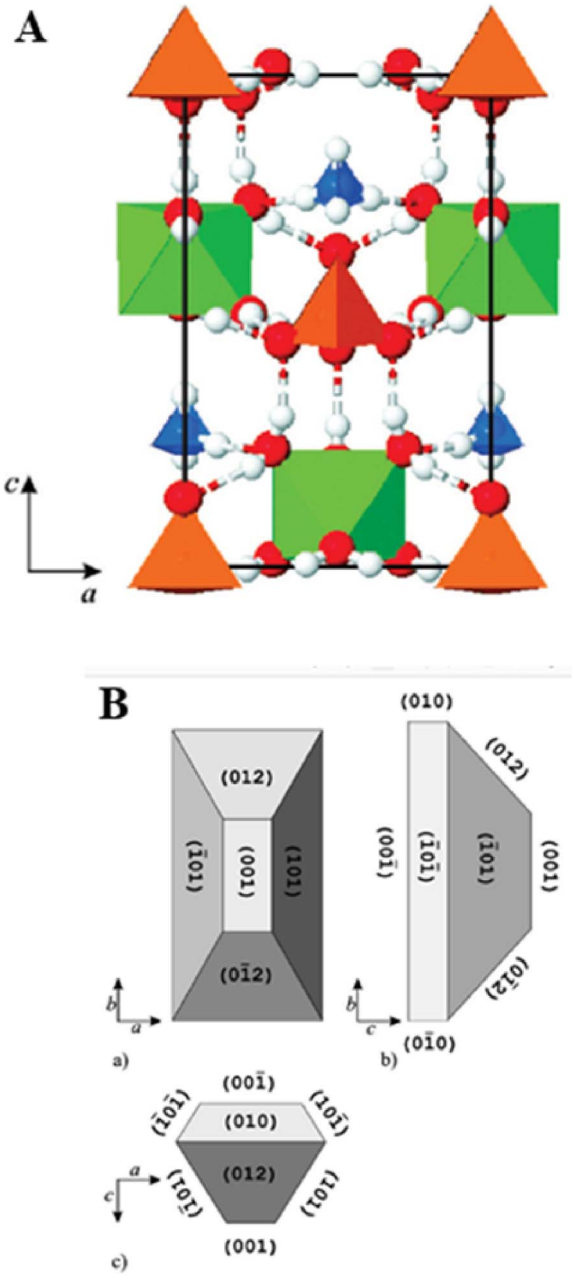

Figure 11. (A) The structure of struvite: PO_4^{3-} and NH_4^+ tetrahedra and $Mg[H_2O]_6^{2+}$ octahedra—orange, blue, and green polyhedra, respectively; O and H atoms—red and white balls, respectively; *c*-axis is polar; plane of observation: (010). (B) Crystallographic faces of struvite crystals (from Prywer *et al.*, 2009 [68]).

values for the crystallographic parameters being $a = b = 9.41844$ Å, $c = 6.88374$ Å [71–77].

Biological apatites have some structural specificities. These arise firstly from the stoichiometric formula which in reality is not the canonical $Ca_{10}(PO_4)_6(OH)_2$ but in practice $Ca_{10-x+u}\square_{x-u}(PO_4)_{6-x}(CO_3)_x(OH)_{2-x+2u}\square_{x-2u}$ where squares correspond to vacancies or additional cations and anions while x and u values are as follows: $0 < x < 2$ and $0 < u < x$. Such complexity takes into account substitution processes [78–80] as well as Ca^{2+} and OH^- vacancies [81,82] (Figure 12B). In the case of biological apatites, the diffraction peak ($hkl = 002$) is sharper than the other peaks, indicating the anisotropy of nanocrystals (needle and/or platelet-like morphology) [83]. Note that a structured hydrated layer exists at the surface of biological apatite which serves as an exchange area with the biological environment (Figure 12C) [84–87].

4.1.3. *Whitlockite*

Whitlockite was named after Herbert Percy Whitlock (1868–1948), a curator of minerals at the American Museum of Natural History in New York (USA). Wk is a complex material which involves cation substitutions, cation vacancies, and protonation of phosphate groups [88–90]. Using quantum chemical structural optimization by Density Functional Theory (DFT) calculations, Debroise *et al.* [90] were able to quantify the ability of Wk to hold these substitutions and vacancies in preferential sites. The impact of Ca^{2+}/Mg^{2+} substitutions on X-ray diffraction (XRD), IR, and Raman characteristics fell within the scope of DFT and compared with experiment. In particular, the crystallographic positions of the vacancy and optimal Ca^{+2}/Mg^{2+} substitution sites were identified (Figure 13). Mg^{2+} concentration could be quantified from the variation in length of the unit cell parameters. Also, they show clearly that Raman spectroscopy is very sensitive to the Mg^{2+} substitutions and to the presence of impurities such as Fe^{2+}. The theoretical IR spectra enabled unequivocal assignment of observed spectral bands to specific vibrations. As with Raman, IR spectra were found to be very sensitive to the presence of defects, and the Mg^{2+} concentration.

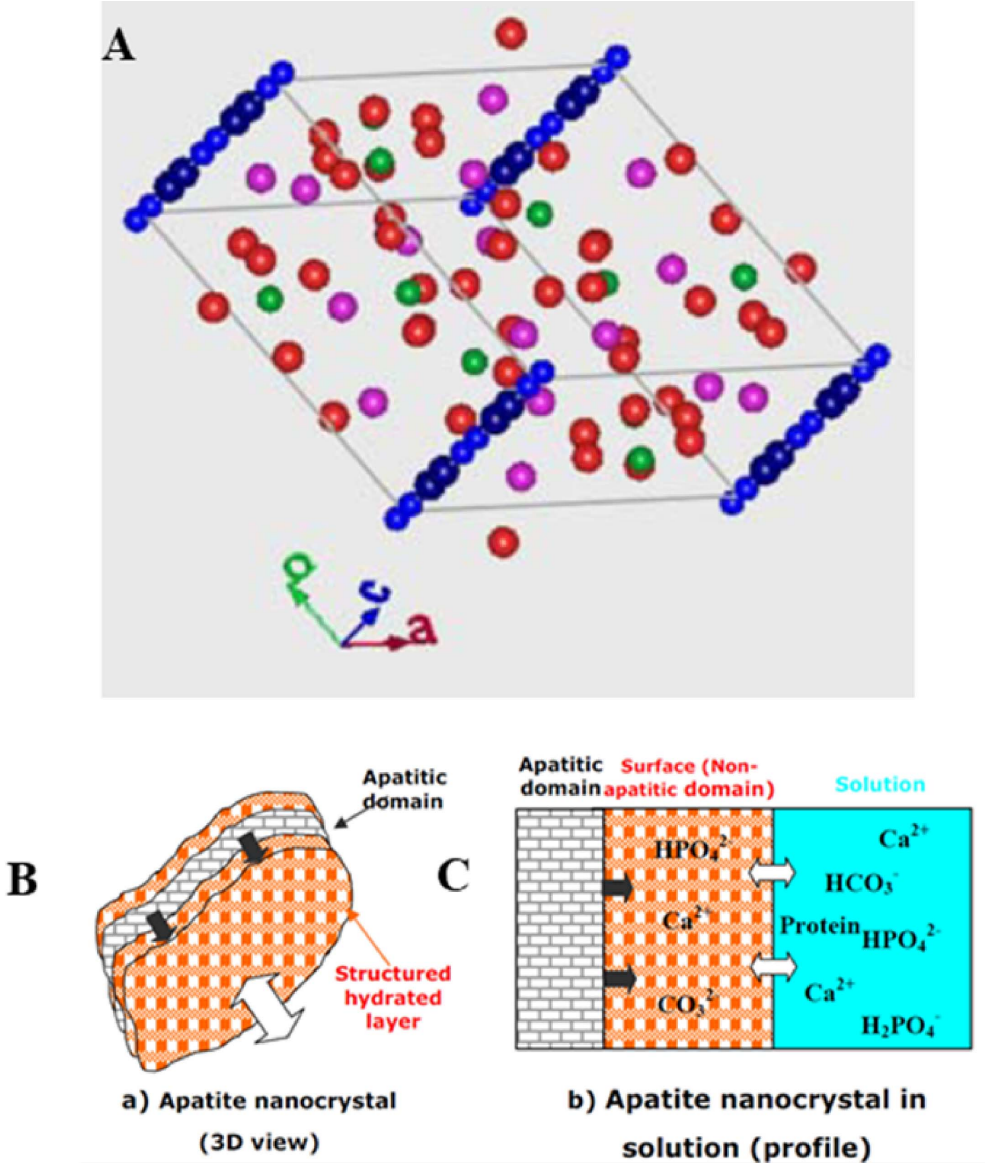

Figure 12. (A) Spatial distribution of different atoms in HAP. Hydrogen and oxygen atoms of the hydroxyl groups represented in blue are located on the *c*-axis. (B) and (C) Schematic model of the surface hydrated layer of poorly crystalline apatite nanocrystals (from Refs. [84,85]).

4.2. *Synthesis of chemical phases related to IKS*

In this section, we will not describe the synthesis of calcium phosphate apatite as its presence in bone has resulted in a considerable literature (see for example [91–97]).

4.2.1. *The case of struvite*

Several papers, arising in two very different research fields, wastewater treatments, and medicine, describe the synthesis of MAP [98–111]. Different precursors have been used in *in vitro* experiments. For example, introduction of Mg^{2+} cations can be performed by addition of $MgSO_4$, $MgCl_2{\cdot}6H_2O$,

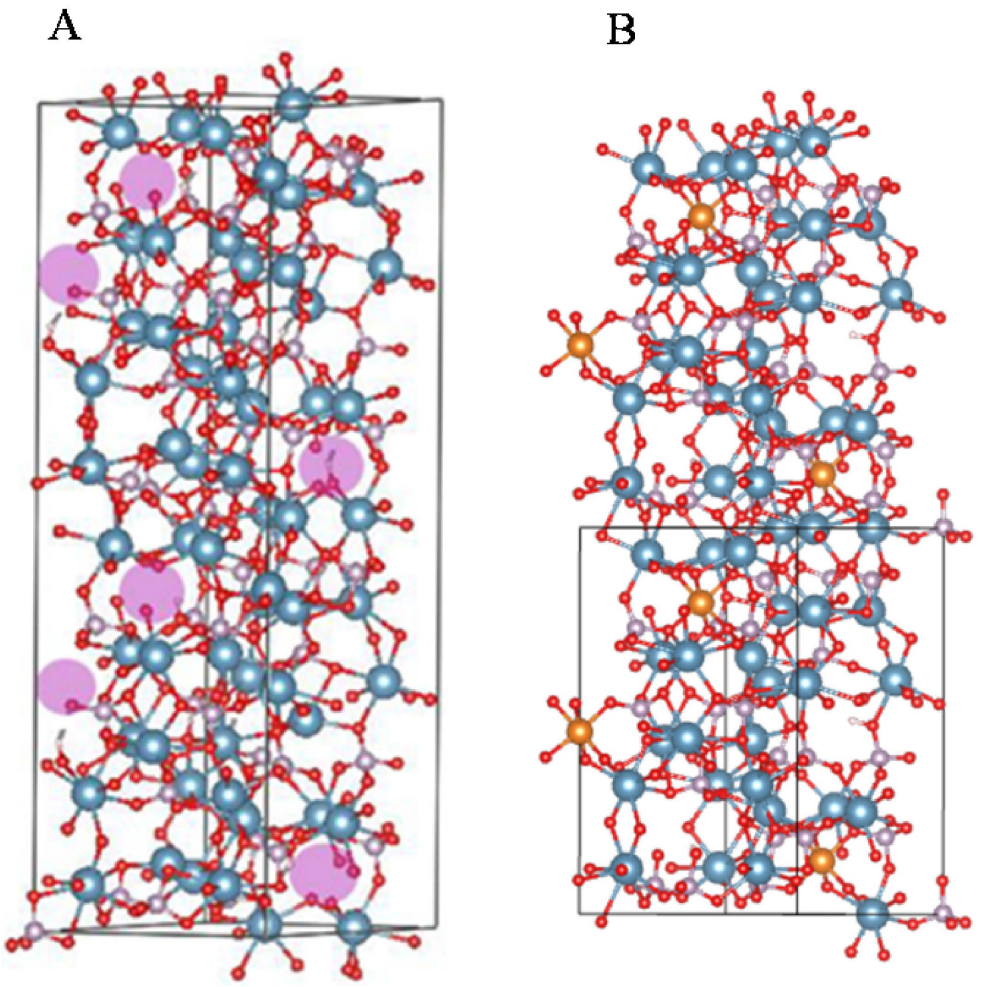

Figure 13. (A) Whitlockite unit cell showing vacancies indicated by purple spheres, which correspond to the crystallographic Ca^{2+} site number 4. (B) Whitlockite unit cell showing the half unit cell with $3Mg^{2+}$ substitutions on the Ca^{2+} sites. Crystallographic site 5 was found to be the most favourable energetically for substitution by Mg^{2+}. Ca: blue, Mg: gold, P: grey, O: red and H: white (from Debroise *et al.* [90]).

$C_4H_6MgO_4$ to the synthesis solution. In the case of Ca^{2+} cations, $CaCl_2{\cdot}2H_2O$ is usually used. Some of these synthetic struvite crystals, such as the one published by Manzoor *et al.* [106], have been obtained in the presence of creatine.

In urine, crystallization of struvite is highly dependent on pH and relative concentrations of magnesium, phosphate and ammonium as shown in Figure 14.

For a similar magnesium ammonium phosphate molar product (pMAP), the relative concentrations of ions involved in pMAP can be very different as shown in Table 4, explaining the fact that bacterial urease activity is not the unique condition for struvite crystallization and that the urine biochemistry of the patient can also be involved (Figure 15). Nevertheless, as shown in Figure 14, urine pH is a very strong determinant for MAP crystallization. Below pH 6.5, the concentrations of magnesium, ammonium, and phosphate, required for MAP formation are too high to correspond to any physiological or pathological condition; this is why MAP in urinary concretions is commonly considered a marker of alkaline urine related to urinary tract infection by urea-splitting bac-

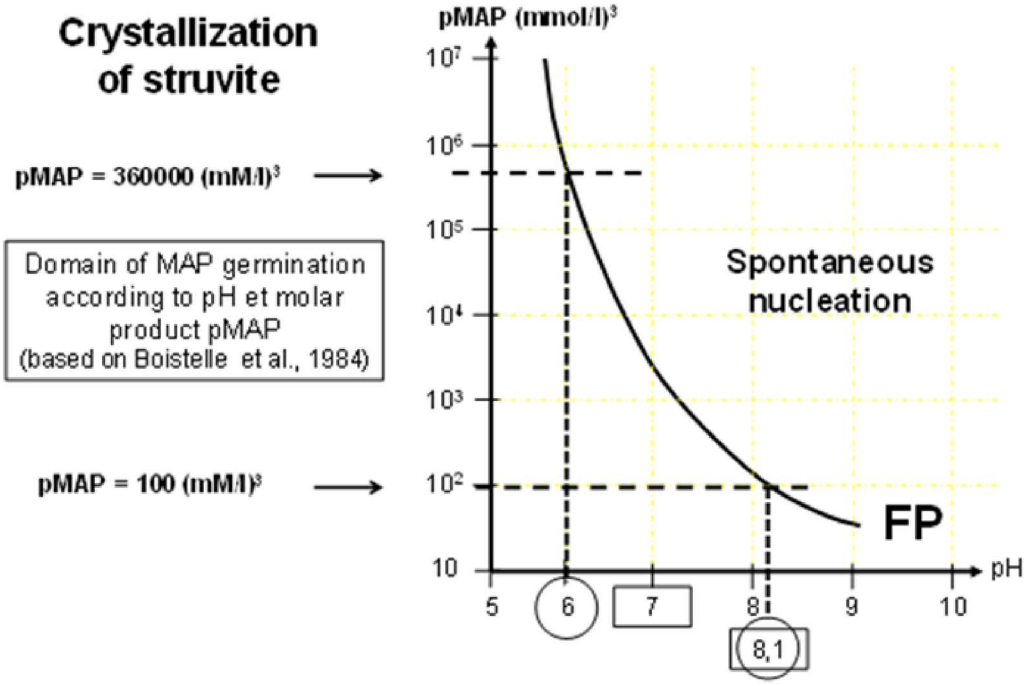

Figure 14. Crystallization of struvite is highly dependent on urine pH. FP is the formation product of MAP, i.e., the limit of pMAP above which MAP crystals spontaneously form in urine.

teria.

As shown in Table 4, the FP for MAP required for crystallization is very high for pH < 6.8 and rarely encountered in urine. In cases of UTI by urea-splitting bacteria, the increase of urine pH by production of NH_3 from urea strongly reduces the pMAP needed for crystallization, mainly encountered in UTI by microorganisms with urease. However, metabolic conditions which allow MAP crystallization without infection should not be ruled out. This might explain the discrepancy between the occurrence of clinically recognized UTI reported by physicians and the presence of MAP in stones although to date no metabolic condition has been clearly identified as a cause of MAP stones without UTI in humans.

However, such conditions have occasionally been reported in animals [111]. Another explanation is related to the time elapsed between stone formation and stone removal. In the absence of clinically recorded UTI with stones that contain MAP, we noted that MAP was mainly located in the nucleus of the stone (89.8% of cases), which could be a marker for a transient episode of UTI.

As shown in Figure 15, the urinary excretion of solutes markedly reflects the risk of crystallization of a given species. For example, in the case of MAP and brushite crystals, and to a lesser extent for ACCP, the excretion of phosphate ions is significantly higher than for other crystalline species, irrespective other parameters such as urine pH.

4.2.2. *The case of whitlockite*

Only a few publications report the synthesis of Wk [113–118], among them note the work of Jang *et al.* introducing a new synthetic route to pure Wk nanocrystals precipitated under Mg^{2+}-rich and physiological conditions [114]. Qi *et al.* [115] generated Wk microspheres which displayed high biocompatibility and an excellent ability to promote adhesion and spreading of MC-3T3 osteoblasts using a novel microwave-assisted method. Also, hydrothermal growth of Wk on a β-TCP surface to enhance osteogenesis has been investigated by Guo *et al.* [116]. Finally, Wk nanoparticles can also be prepared by precipitation using calcium hydroxide and magnesium hydroxide [117].

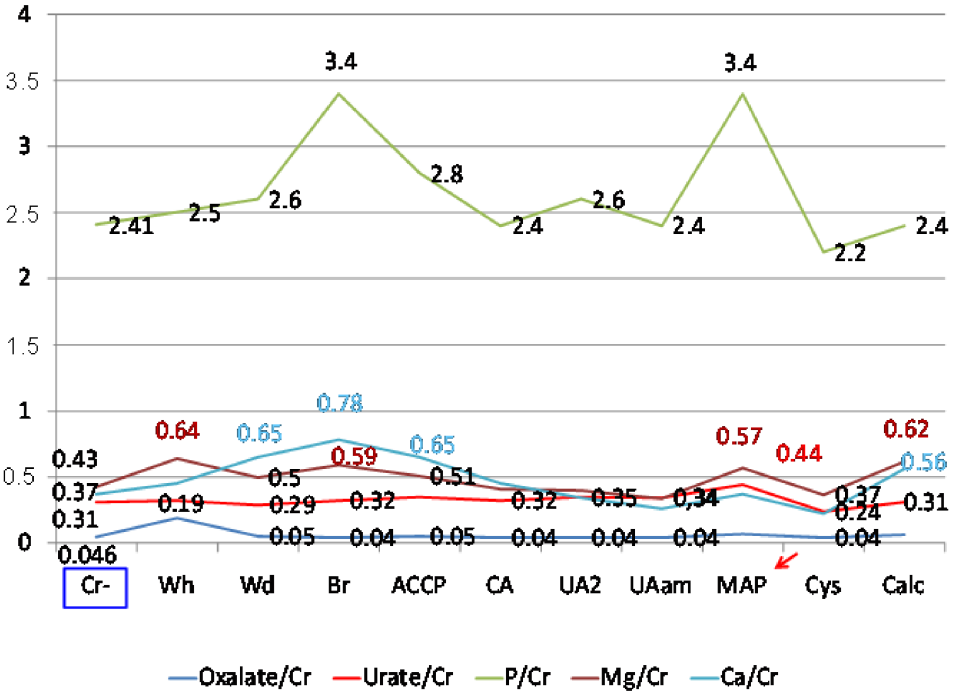

Figure 15. On the *y* axis, are shown the mean values of oxalate to creatinine ratio (—), urate to creatinine ratio (—), phosphate to creatinine ratio (—), magnesium to creatinine ratio (—) and calcium to creatinine ratio (—) for the different crystalline phases described below. Cr^{-} = absence of crystals. Crystalline phases: Wh = whewellite; Wd = weddellite; Br = brushite; ACCP = amorphous carbonated calcium phosphate; CA = carbapatite; UA2 = uric acid dihydrate; UAam = uric acid amorphous; MAP = struvite; Cys = cystine; Calc = calcite.

Recently, Wang *et al.* [118] have developed an interesting synthesis of Wk nanocrystals using a tri-solvent system for the solid–liquid–solution process, which offers the opportunity to generate Wk nanocrystals with tuneable size, morphology (nanoplates, nanospheres), and surface properties (hydrophobic, hydrophilic), impossible to achieve using the traditional precipitation method.

Regarding the role of pH in the synthesis of Wk, it is worth underlining that, as noted by Jang *et al.* [114], Wk had greater stability than HAP in acidic conditions below pH 4.2. These authors also confirmed that calcium phosphate apatite can directly transform into Wk under appropriate acidic pH conditions with a sufficient Mg^{2+} cations content in the medium.It is notable that, in urinary stones, Wk has occurred mixed with MAP in 11.3% of cases and that a mixture of WK and MAP was found in the same layers of more than 100 stones, suggesting that acidic conditions are not required for Wk formation under biological conditions.

4.3. *Crystallite morphology of chemical phases related to IKS*

4.3.1. *Morphology of MAP crystallites*

Various publications have reported the morphology of MAP crystallites [112,119]. Prywer *et al.* [112] have used scanning electron microscopy to correlate crystal morphology with the pH of artificial urine (Figure 16).

As shown by Daudon and Frochot [120], MAP is highly dependent on urinary pH and may occur in a range between 6.8 and 9.0 (Figure 17).

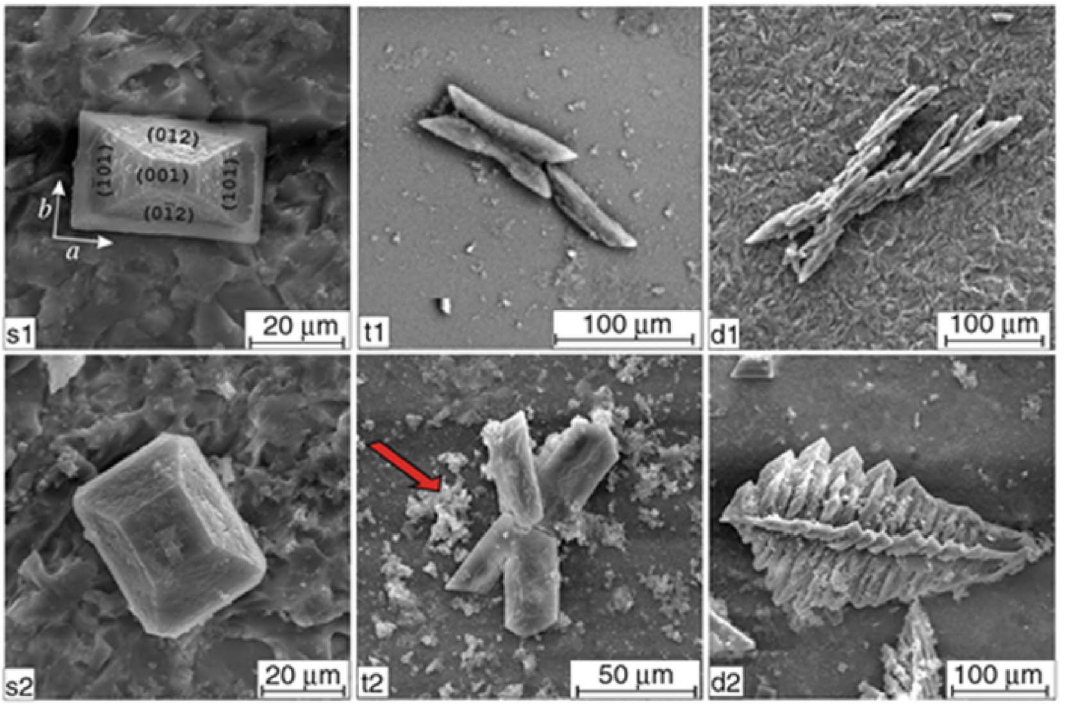

Figure 16. SEM micrographs illustrating the dependence of morphology and habits of struvite on pH of artificial urine; left column: single hemimorphic crystals obtained at pH range 7.2–9.0; middle column: contact (t1) and penetration (t2) twins obtained at pH range 9.0–9.5; right column: X-shaped (d1) and fern-leaf (d2) dendritic crystals obtained at the highest pH values (pH 9.5); arrow indicates CA precipitation (from Prywer *et al.* [112]).

At this point, it is worth underlining those bacteria are able to affect and modify the dimensions or the morphology of MAP crystals [112,119–123]. For example, the results of Sun *et al.* [123] show that MAP particles produced in the presence of bacteria are larger than in the absence. It is possible that bacterial biomolecules may act as templates to induce the nucleation, growth, and aggregation of struvite crystals.

4.3.2. *Morphology of CA and Wk crystallites*

Several investigators have reported the presence of bacterial imprints in renal stones using transmission and scanning electron microscopy [124–126]. Indeed, this approach may help identify bacteria that may contribute to stone formation, even though urine culture results might be negative.

More specifically, it was reported that in IKS bacterial imprints are only observed on areas composed of CA and not on MAP crystals [127], as has also been observed in IKS containing Wk (Figure 18). In a contribution to this special issue we have shown that Wk crystallites display a specific morphology [32].

5. Conclusions and perspectives

The comprehensive set of clinical and physicochemical data presented in this contribution shows clearly that IKS display a complex chemistry which is clearly not limited to struvite. For the clinician, such chemical complexity calls for a precise analysis of different infrared spectra related to the core and the surface of a kidney stone. With the increase of bacterial antibiotic resistance and the paucity of new antibiotics (as underlined by the World Health Organization),[1] it is

[1] https://www.who.int/news/item/17-01-2020-lack-of-new-antibiotics-threatens-global-efforts-to-contain-drug-resistant-infections.

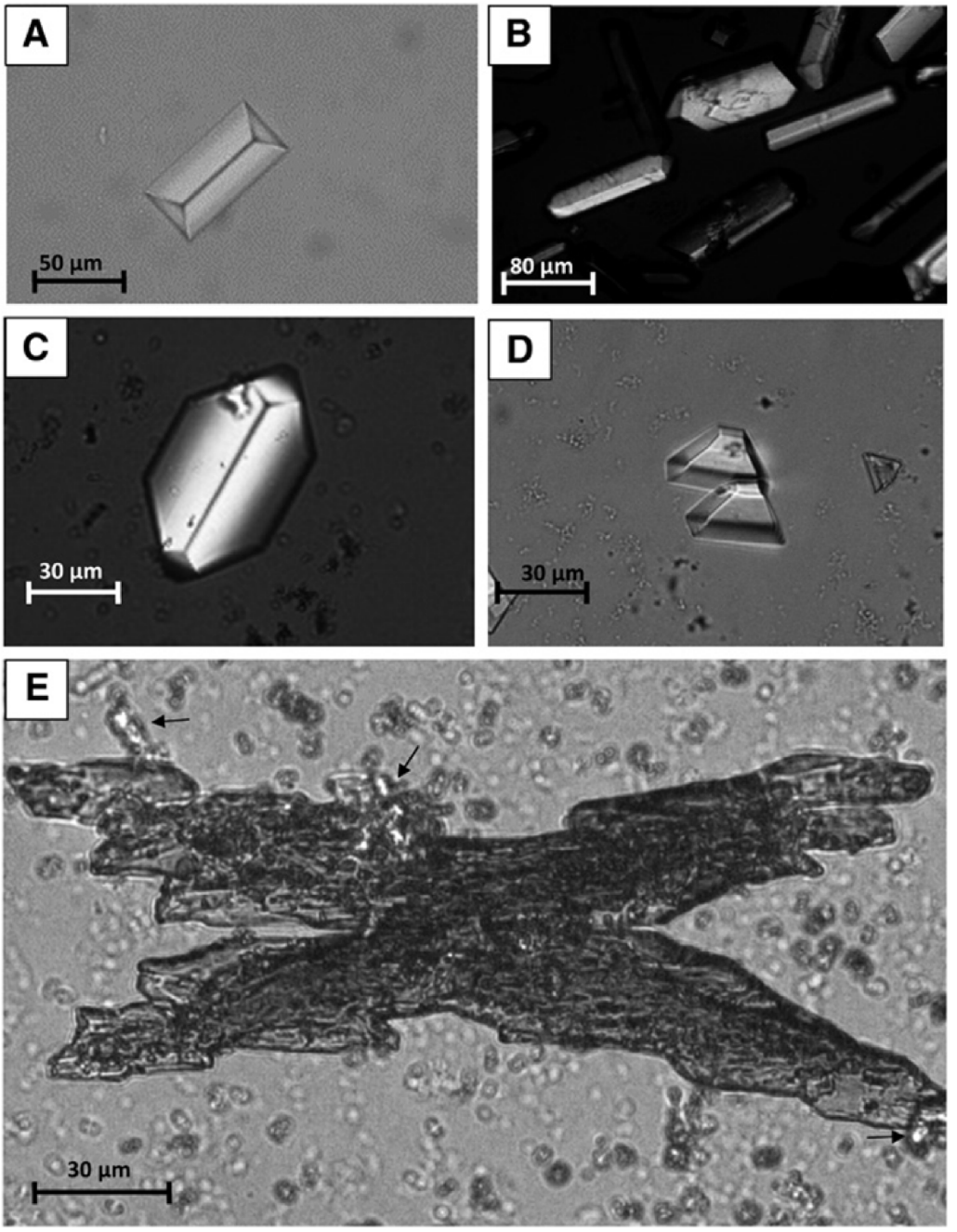

Figure 17. MAP crystals as seen under polarized light (from Daudon and Frochot, 2015 [120]). (A) A coffin-shaped crystal of MAP. (B) Rod-shaped and coffin-shaped crystals of MAP. (C) A hexagonal crystal of MAP and small agglomerates of amorphous carbonated calcium phosphate grains. (D) Trapezoidal crystals of MAP. (E) A large X-shaped dendritic crystal of MAP with birefringent small aggregates of ammonium hydrogen urate crystals (black arrows).

Table 4. Formation product (FP) for MAP (pMAP) at different urinary pH and ion concentrations (adapted from Boistelle *et al.* 1984 [110])

Ion concentration (mmol/L)			Formation product (FP) of pMAP ($\mu mol/L^3$)	pH at FP
Mg	PO_4	NH_4		
1	5	10	50	8.7
1	10	15	150	8.0
1	10	50	500	7.45
2	20	20	800	7.3
3	20	30	1800	6.95
2	10	100	2000	7.0
2	100	10	2000	7.0
4	30	30	3600	6.8
6	30	40	7200	6.75
3	10	300	9000	6.7
7	30	50	10,500	6.65
7	40	80	22,400	6.5
7	50	100	35,000	6.4
7	100	200	140,000	6.15
8	150	300	360,000	6.0

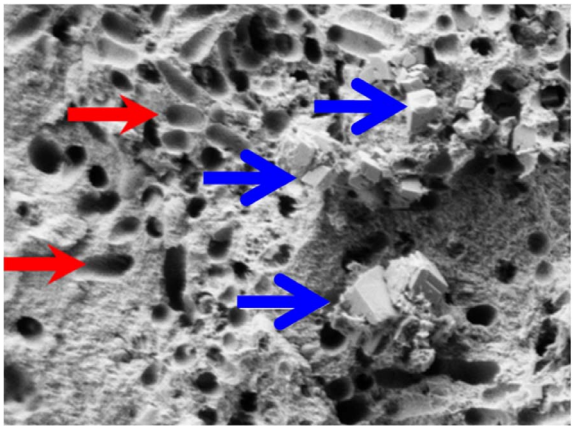

Figure 18. SEM image showing bacterial imprints (red arrows) in a stone made of whitlockite (blue arrows) mixed with carbapatite.

quite clear that IKS constitute a major topic of interest for the medical community. It is thus of primary importance to accurately detect the presence of MAP and Wk in urinary stones as well as to precisely measure the carbonation rate of calcium phosphate apatite by FTIR spectroscopy.

Conflicts of interest

Authors have no conflict of interest to declare.

References

[1] W. E. Stamm, S. R. Norrby, *J. Infect. Dis.*, 2001, **183**, S1-S4.
[2] B. Foxman, *Infect. Dis. Clin. North Am.*, 2014, **28**, 1-13.
[3] A. L. Flores-Mireles, J. N. Walker, M. Caparon, S. J. Hultgren, *Nat. Rev. Microbiol.*, 2015, **13**, 269-284.
[4] A. E. Krambeck, N. F. Khan, M. E. Jackson, J. E. Lingeman, J. A. McAteer, J. C. Williams, *J. Urol.*, 2010, **184**, 1543-1549.
[5] R. Flannigan, W. H. Choy, B. Chew, D. Lange, *Nat. Rev. Urol.*, 2014, **11**, 333-341.
[6] J. Prywer, M. Olszynski, *Curr. Med. Chem.*, 2017, **24**, 292-311.
[7] W. L. Strohmaier, "Infection induced urinary stones. Version: 2018-02-27", in *Urogenital Infections and Inflammations* (T. E. Bjerklund Johansen, F. M. E. Wagenlehner, T. Matsumoto, Y. H. Cho, J. N. Krieger, D. Shoskes, K. G. Naber, eds.), German Medical Science GMS Publishing House, Duesseldorf, 2017.
[8] J. L. Bauza, E. C. Pieras, F. Grases, V. Tubau, J. Guimerà, X. A. Sabaté, P. Pizà, *Med. Hypotheses*, 2018, **118**, 34-35.
[9] E. J. Espinosa-Ortiz, B. H. Eisner, D. Lange, R. Gerlach, *Nat. Rev. Urol.*, 2019, **16**, 35-53.
[10] D. W. L. Hukins, D. S. Hickey, A. P. Kennedy, *Br. J. Urol.*, 1983, **55**, 304-305.
[11] D. Stickler, L. Ganderton, J. King, J. Nettleton, C. Winters, *Urol. Res.*, 1993, **21**, 407-411.

[12] D. J. Stickler, *J. Intern. Med.*, 2014, **276**, 120-129.

[13] C. E. Chenoweth, C. V. Gould, S. Saint, *Infect. Dis. Clin. North Am.*, 2014, **28**, 105-119.

[14] R. Golan, K. L. Cooper, O. Shah, *Rev. Urol.*, 2020, **22**, 52-56.

[15] N. Karki, S. W. Leslie, "Struvite and triple phosphate renal calculi. [Updated 2021 Aug. 12]", in *StatPearls [Internet]*, StatPearls Publishing, Treasure Island (FL), 2021.

[16] E. Letavernier, "Quel est le profil métabolique des patients qui développent des calculs d'infection ? Calculs infectieux sans struvite", in *Communication aux 20*émes *Confrontations Clinico-Biologiques sur la Lithiase Urinaire* (Paris, France), 2015.

[17] R. Miano, S. Germani, G. Vespasiani, *Urol. Int.*, 2007, **79**, 32-36.

[18] M. Daudon, M. Livrozet, D. Bazin, J. P. Haymann, E. Letavernier, "Proceedings of the 24e Confrontations Clinico-Biologiques sur la Lithiase Urinaire" (Paris, France), 2019, 8-18.

[19] D. Bazin, M. Daudon, *Ann. Biol. Clin.*, 2015, **73**, 517-534.

[20] M. Daudon, B. Bounxouei, F. Santa Cruz, S. Leite da Silva, B. Diouf, F. F. Angwafoo 3rd, J. Talati, G. Desrez, *Prog. Urol.*, 2004, **14**, 1151-1161.

[21] M. Daudon, J. C. Doré, B. Lacour, *Urol. Res.*, 2004, **32**, 241-247.

[22] R. Moses, V. M. Pais Jr., M. Ursiny, E. L. Prien Jr., N. Miller, B. H. Eisner, *Urolithiasis*, 2015, **43**, 135-139.

[23] D. L. Lamm, S. A. Johnson, A. M. Friedlander, R. F. Gittes, *Urology*, 1977, **10**, 418-421.

[24] D. P. Griffith, *Kidney Int.*, 1978, **13**, 372-382.

[25] D. P. Griffith, *Urol. Res.*, 1979, **7**, 215-221.

[26] M. I. Resnick, *Urol. Clin. North Am.*, 1981, **8**, 265-276.

[27] S. P. Lerner, M. J. Gleeson, D. P. Griffith, *J. Urol.*, 1989, **141**, 753-758.

[28] T. D. Cohen, G. M. Preminger, *Semin. Nephrol.*, 1996, **16**, 425-434.

[29] J. S. Rodman, *Nephron*, 1999, **81**, 50-59.

[30] J. C. Williams Jr., A. J. Sacks, K. Englert, R. Deal, T. L. Farmer, M. E. Jackson, J. E. Lingeman, J. A. McAteer, *J. Endourol.*, 2012, **26**, 726-731.

[31] L. Maurice-Estepa, P. Levillain, B. Lacour, M. Daudon, *Scand. J. Urol. Nephrol.*, 1999, **33**, 299-305.

[32] D. Bazin, R. J. Papoular, E. Elkaim, R. Weil, D. Thiaudière, C. Pisapia, B. Ménez, N. S. Hwang, F. Tielens, M. Livrozet, E. Bouderlique, J.-P. Haymann, E. Letavernier, L. Hennet, V. Frochot, M. Daudon, *C. R. Chimie*, 2022, **25**, no. S1, 343-354.

[33] X. Carpentier, M. Daudon, O. Traxer, P. Jungers, A. Mazouyes, G. Matzen, E. Véron, D. Bazin, *Urology*, 2009, **73**, 968-975.

[34] M. Daudon, H. Bouzidi, D. Bazin, *Urol. Res.*, 2010, **38**, 459-467.

[35] K. M. Englert, J. A. McAteer, J. E. Lingeman, J. C. Williams Jr., *Urolithiasis*, 2013, **41**, 389-394.

[36] M. Daudon, C. A. Bader, P. Jungers, *Scan. Microsc.*, 1993, **7**, 1081-1104.

[37] M. Daudon, A. Dessombz, V. Frochot, E. Letavernier, J.-P. Haymann, P. Jungers, D. Bazin, *C. R. Chim.*, 2016, **19**, 1470-1491.

[38] A. Hesse, H.-G. Tiselius, A. Jahnen (eds.), *Urinary Stones*, Karger, Basel, 2002.

[39] Y.-H. Chou, C.-N. Huang, W.-M. Li, S.-P. Huang, W.-J. Wu, C.-C. Tsai, A.-W. Chang, S.-M. Chen, Y.-L. Lin, Y.-P. Lin, *Kaohsiung J. Med. Sci.*, 2012, **28**, 259-264.

[40] C. Poulard, A. Dessombz, M. Daudon, D. Bazin, *C. R. Chim.*, 2016, **19**, 1597-1604.

[41] E. Van de Perre, G. Reichman, D. De Geyter, C. Geers, K. M. Wissing, E. Letavernier, *Front. Med.*, 2020, **7**, article no. 609024.

[42] P. Calvó, J. L. Bauza, F. Julià, J. Guimerá, E. C. Pieras, A. Costa-Bauzá, F. Grases, *C. R. Chimie*, 2022, **25**, no. S1, 425-430.

[43] A. Trinchieri, *Urologia*, 2014, **81**, 93-98.

[44] E. L. Prien, *Clin. Microbiol. Newslett.*, 1990, **12**, 129-132.

[45] I. Konieczna, P. Żarnowiec, M. Kwinkowski, B. Kolesińska, J. Frączyk, Z. Kamiński, W. Kaca, *Curr. Protein Pept. Sci.*, 2012, **13**, 789-806.

[46] H. L. T. Mobley, M. D. Island, R. P. Hausinger, *Microbiol. Rev.*, 1995, **59**, 451-480.

[47] K. H. Bichler, E. Eipper, K. Naber, V. Braun, R. Zimmermann, S. Lahme, *Int. J. Antimicrob. Ag.*, 2002, **19**, 488-498.

[48] B. Wiedemann, A. Heisig, P. Heisig, *Antibiotics*, 2014, **3**, 341-352.

[49] J. D. Sobel, D. Kaye *et al.*, "Chapter 74—Urinary tract infections", in *Mandell, Douglas, and Bennett's Principles and Practice of Infectious Diseases* (J. E. Bennett *et al.*, eds.), Elsevier, Philadelphia, 8th ed., 2015, 886-913.e3.

[50] Y. M. Romanova, N. S. Mulabaev, E. R. Tolordava, A. V. Seregin, I. V. Seregin, N. V. Alexeeva, T. V. Stepanova, G. A. Levina, O. I. Barhatova, N. A. Gamova, S. A. Goncharova, L. V. Didenko, I. V. Rakovskaya, *Mol. Genet. Mikrobiol. Virol.*, 2015, **2**, 20-25.

[51] M. Gajdács, M. Ábrók, A. Lázár, K. Burián, *Sci. Rep.*, 2020, **10**, article no. 17658.

[52] N. Quy Dao, M. Daudon, *Infrared and Raman Spectra of Calculi*, Elsevier, Paris, 1997.

[53] L. M. Estepa, P. Levillain, B. Lacour, M. Daudon, *Clin. Chem. Lab. Med.*, 1999, **37**, 1043-1052.

[54] F. Cohen-Solal, B. Dabrowsky, J. C. Boulou, B. Lacour, M. Daudon, *Appl. Spectrosc.*, 2004, **58**, 671-678.

[55] D. Bazin, M. Daudon, "Nouvelles Méthodes d'étude des calculs et plaques de Randall", in *Actualités néphrologiques Jean Hamburger* (P. Lesavre, T. Drüeke, C. Legendre, P. Niaudet, eds.), Flammarion — Médecine, Paris, 2010, 75-98.

[56] M. Daudon, D. Bazin, "New techniques to characterize kidney stones and Randall's plaque", in *Urolithiasis: Basic Science and Clinical Practice* (J. J. Talati, H. G. Tiselius, D. M. Albala, Z. Ye, eds.), Springer, London, 2012, 683-707.

[57] D. Bazin, J.-P. Haymann, E. Letavernier, J. Rode, M. Daudon, *Presse Med.*, 2014, **43**, 135-148.

[58] M. L. Giannossi, *J. X-ray Sci. Technol.*, 2015, **23**, 401-407.

[59] M. Daudon, D. Bazin, *C. R. Chim.*, 2016, **19**, 1416-1423.

[60] D. Bazin, E. Letavernier, J.-P. Haymann, P. Méria, M. Daudon, *Prog. Urol.*, 2016, **26**, 608-618.

[61] D. Sidorczuk, M. Kozanecki, B. Civalleri, K. Pernal, J. Prywer, *J. Phys. Chem. A*, 2020, **124**, 8668-8678.

[62] K. Suguna, M. Thenmozhi, C. Sekar, *Bull. Mater. Sci.*, 2012, **35**, 701-706.

[63] C. Rey, M. Shimizu, B. Collins, M. J. Glimcher, *Calcif. Tissue Int.*, 1990, **46**, 384-394.

[64] M. E. Fleet, *Am. Mineral.*, 2017, **102**, 149-157.

[65] A. Whitaker, J. W. Jeffery, *Acta Crystallogr. B*, 1970, **26**, 1429-1440.
[66] F. Abbona, R. Boistelle, *J. Cryst. Growth*, 1979, **46**, 339-354.
[67] G. Ferraris, H. Fuess, W. Joswig, *Acta Crystallogr. B*, 1986, **42**, 253-258.
[68] J. Prywer, A. Torzewska, *Cryst. Growth Des.*, 2009, **9**, 3538-3543.
[69] Z. Romanowski, P. Kempisty, J. Prywer, S. Krukowski, A. Torzewska, *J. Phys. Chem. A*, 2010, **114**, 7800-7808.
[70] J. Prywer, L. Siero, A. Czylkowska, *Crystals*, 2019, **9**, article no. 89.
[71] S. Naray-Szabo, *Z. Kristallogr. Kristallgeom. Kristallphys. Kristall Chem.*, 1930, **75**, 387-398.
[72] J. C. Elliot, P. E. Mackie, R. A. Young, *Science*, 1973, **180**, 1055-1057.
[73] J. C. Elliot, E. Dykes, P. E. Mackie, *Acta Crystallogr. B*, 1981, **37**, 435-438.
[74] J. C. Elliot, *Structure and Chemistry of the Apatites and Other Calcium Orthophosphates*, Elsevier, Amsterdam, 1994.
[75] T. J. White, D. Zhi Li, *Acta Crystallogr. B*, 2003, **59**, 1-16.
[76] M. Vallet-Reg, M. J. Gonzalez-Calbet, *Prog. Solid State Chem.*, 2004, **32**, 1-31.
[77] D. Bazin, C. Chappard, C. Combes, X. Carpentier, S. Rouzière, G. André, G. Matzen, M. Allix, D. Thiaudière, S. Reguer, P. Jungers, M. Daudon, *Osteoporos Int.*, 2009, **20**, 1065-1075.
[78] Y. Suetsugu, Y. Takahashi, F. P. Okamura, J. Tanaka, *J. Solid State Chem.*, 2000, **155**, 292-297.
[79] T. Tite, A.-C. Popa, L. M. Balescu, I. M. Bogdan, I. Pasuk, J. M. F. Ferreira, G. E. Stan, *Materials (Basel)*, 2018, **11**, article no. 2081.
[80] Y. Jiang, Z. Yuan, J. Huang, *Mater. Technol.*, 2020, **35**, 785-796.
[81] C. Rey, J. L. Miquel, L. Facchini, A. P. Legrand, M. J. Glimcher, *Bone*, 1995, **16**, 583-586.
[82] C. K. Loong, C. Rey, L. T. Kuhn, C. Combes, Y. Wu, S. H. Chen, M. J. Glimcher, *Bone*, 2000, **26**, 599-602.
[83] H. M. Kim, C. Rey, M. J. Glimcher, *J. Bone Miner. Res.*, 1995, **10**, 1589-1601.
[84] C. Combes, S. Cazalbou, C. Rey, *Minerals*, 2016, **6**, article no. 34.
[85] D. Eichert, C. Drouet, H. Sfihi, C. Rey, C. Combes, *Nanocrystalline Apatite Based Biomaterials: Synthesis, Processing and Characterization*, Nova Science Publishers Inc., New York, NY, USA, 2009.
[86] J. Gómez-Morales, M. Iafisco, J. M. Delgado-López, S. Sarda, C. Drouet, *Prog. Cryst. Growth Character. Mater.*, 2013, **59**, 1-46.
[87] C. Drouet, M. Aufray, S. Rollin-Martinet, N. Vandecandelaère, D. Grossin, F. Rossignol, E. Champion, A. Navrotsky, C. Rey, *Am. Mineral.*, 2018, **103**, 550-564.
[88] C. Calco, R. Gopal, *Am. Mineral.*, 1975, **60**, 120-133.
[89] H. L. Jang, K. Jin, J. Lee, K. Kim, S. H. Nahm, K. S. Hong, K. T. Nam, *ACS Nano*, 2014, **8**, 634-641.
[90] T. Debroise, E. Colombo, G. Belletti, J. Vekeman, Y. Su, R. Papoular, N. S. Hwang, D. Bazin, M. Daudon, P. Quaino, F. Tielens, *Cryst. Growth Des.*, 2020, **20**, 2553-2561.
[91] S. I. Stupp, G. W. Ciegler, *J. Biomed. Mater. Res.*, 1992, **26**, 169-183.
[92] B. Viswanath, N. Ravishankar, *Biomaterials*, 2008, **29**, 4855-4863.
[93] Y. Wang, S. Von Euw, F. M. Fernandes, S. Cassaignon, M. Selmane, G. Laurent, G. Pehau-Arnaudet, C. Coelho, L. Bonhomme-Coury, M.-M. Giraud-Guille, F. Babonneau, T. Azaïskofina, N. Nassif, *Nat. Mater.*, 2013, **12**, 1144-1153.
[94] C. Combes, C. Rey, *Acta Biomater.*, 2010, **6**, 3362-3378.
[95] N. Nassif, F. Martineau, O. Syzgantseva, F. Gobeaux, M. Willinger, T. Coradin, S. Cassaignon, T. Azaïs, M. M. Giraud-Guille, *Chem. Mater.*, 2010, **22**, 3653-3663.
[96] C. Rey, C. Combes, C. Drouet, S. Cazalbou, D. Grossin, F. Brouillet, S. Sarda, *Progr. Cryst. Growth Character. Mater.*, 2014, **60**, 63-73.
[97] D. P. Minh, N. D. Tran, A. Nzihou, P. Sharrock, *Mater. Res. Bull.*, 2014, **51**, 236-243.
[98] S. Shaddel, S. Ucar, J.-P. Andreassen, S. W. Østerhu, *J. Environ. Chem. Eng.*, 2019, **7**, article no. 102918.
[99] A. Capdevielle, E. Sorová, B. Biscans, F. Béline, M.-L. Daumer, *J. Hazard. Mater.*, 2013, **244–245**, 357-369.
[100] H. Li, Q.-Z. Yao, Y.-Y. Wang, Y.-L. Li, G.-T. Zhou, *Sci. Rep.*, 2015, **5**, article no. 7718.
[101] B. Suyamud, J. Ferrier, L. Csetenyi, D. Inthorn, G. M. Gadd, *Environ. Microb.*, 2020, **22**, 1588-1602.
[102] S. Sutiyono, L. Edahwati, D. S. Perwitasari, S. Muryanto, J. Jamari, A. P. Bayuseno, *MATEC Web Conf.*, 2016, **58**, article no. 01006.
[103] V. V. Vol'khin, D. A. Kazakov, G. V. Leont'eva, Y. V. Andreeva, E. A. Nosenko, M. Y. Siluyanova, *Russ. J. Appl. Chem.*, 2015, **88**, 1986-1996.
[104] H. Li, Q.-Z. Yao, S.-H. Yu, Y.-R. Huang, X.-D. Chen, S.-Q. Fu, G.-T. Zhou, *Am. Mineral.*, 2017, **102**, 381-390.
[105] B. Tansel, G. Lunn, O. Monje, *Chemosphere*, 2018, **194**, 504-514.
[106] M. A. P. Manzoor, M. Mujeeburahiman, S. R. Duwal, P. D. Rekha, *Biocatal. Agricult. Biotechnol.*, 2019, **17**, 566-570.
[107] D. Kim, C. Olympiou, C. P. McCoy, N. J. Irwin, J. D. Rimer, *Chemistry*, 2020, **26**, 3555-3563.
[108] A. N. Kofina, P. G. Koutsoukos, *Cryst. Growth Des.*, 2005, **5**, 489-496.
[109] H. Li, Q.-Z. Yao, Z.-M. Dong, T.-L. Zhao, G.-T. Zhou, S.-Q. Fu, *ACS Sustain. Chem. Eng.*, 2019, **7**, 2035-2043.
[110] R. Boistelle, F. Abbona, Y. Berland, M. Granvuillemin, M. Olmer, *Nephrologie*, 1984, **5**, 217-221.
[111] G. Sanders, A. Hesse, D. B. Leusmann, *Scan. Electron Microsc.*, 1986, **4**, 1713-1720.
[112] J. Prywer, A. Torzewska, T. Plocinski, *Urol. Res.*, 2012, **40**, 699-707.
[113] S. Rowles, *Bull. Soc. Chim. Fr.*, 1968, 1798-1802.
[114] H. L. Jang, H. K. Lee, K. Jin, H.-Y. Ahn, H.-E. Lee, K. T. Nam, *J. Mater. Chem. B*, 2015, **3**, 1342-1349.
[115] C. Qi, Y.-J. Zhu, F. Chen, J. Wu, *J. Mater. Chem. B*, 2015, **3**, 7775-7786.
[116] X. Guo, X. Liu, H. Gao, X. Shi, N. Zhao, Y. Wang, *J. Mater. Sci. Technol.*, 2017, **34**, 1054-1059.
[117] N. S. M. Pillai, K. Eswar, S. Amirthalingam, U. Mony, P. K. Varma, R. Jayakumar, *ACS Appl. Biomater.*, 2019, **2**, 865-873.
[118] C. Wang, K.-J. Jeong, H. J. Park, M. Lee, S.-C. Ryu, D. Y. Hwang, K. H. Namb, I. H. Han, J. Lee, *J. Colloid Interface Sci.*, 2020, **569**, 1-11.
[119] J. Prywer, A. Torzewska, *Cryst. Res. Technol.*, 2009, **45**, 1283-1289.

[120] M. Daudon, V. Frochot, *Clin. Chem. Lab. Med.*, 2015, **53**, S1479-S1487.
[121] R. R. Sadowski, J. Prywer, A. Torzewska, *Cryst. Res. Technol.*, 2014, **49**, 478-489.
[122] A. Sinha, A. Singh, S. Kumar, S. K. Khare, A. Ramanan, *Water Res.*, 2014, **54**, 33-43.
[123] J. Sun, L. Chen, X. Wang, S. Cao, W. Fu, W. Zheng, *Chemistry*, 2012, **42**, 445-448.
[124] L. CifuentesDelatte, M. Santos, *Eur. Urol.*, 1977, **3**, 96-99.
[125] L. CifuentesDelatte, *Composicion y estructura de los calculosrenales*, Ed. Salvat, Barcelona, 1984.
[126] D. B. Leusmann, *Pathog. Klin. Harnsteine*, 1982, **8**, 275-280.
[127] D. Bazin, G. André, R. Weil, G. Matzen, E. Véron, X. Carpentier, M. Daudon, *Urology*, 2012, **79**, 786-790.